Multipath Ghosts in Through-the-Wall Radar Imaging: Challenges and Solutions

Abdi T. Abdalla, Mohammad T. Alkhodary, and Ali H. Muqaibel

In through-the-wall radar imaging (TWRI), the presence of front and side walls causes multipath propagation, which creates fake targets called multipath ghosts. They populate the scene and reduce the probability of correct target detection, classification, and localization. In modern TWRI, specular multipath exploitation has received considerable attention for reducing the effects of multipath ghosts. However, this exploitation is challenged by the requirements of the reflecting geometry, which is not always available. Currently, the demand for a high radar image resolution dictates the use of a large aperture and wide bandwidth. This results in a large amount of data. To tackle this problem, compressive sensing (CS) is applied to TWRI. With CS, only a fraction of the data are used to produce a high-quality image, provided that the scene is sparse. However, owing to multipath ghosts, the scene sparsity is highly deteriorated; hence, the performance of the CS algorithms is compromised. This paper presents and discusses the adverse effects of multipath ghosts in TWRI. It describes the physical formation of ghosts, their challenges, and existing suppression techniques.

Keywords: Aspect dependence, Compressive sensing, Multipath ghost, Subaperture, Through-the-wall radar imaging.

Manuscript received Nov. 20, 2017; revised Jan. 19, 2018; accepted Apr. 9, 2018.

Abdi T. Abdalla (abdit@udsm.ac.tz) is with the Department of Electronics and Telecommunication Engineering, University of Dar es Salaam, Tanzania.

Mohammad T. Alkhodary (corresponding author, mohamd2020@hotmail.com) and Ali H. Muqaibel (muqaibel@kfupm.edu.sa) are with the Electrical Engineering Department, King Fahd University of Petroleum and Minerals, Dhahran, Saudi Arabia.

I. Introduction

Through-the-wall radar imaging (TWRI) is an emerging technology that facilitates the detection, classification, and localization of targets from behind obstacles or walls using electromagnetic (EM) waves. Radar mainly relies on the time delay to localize a given target. The time delay is defined as the time elapsed when an EM wave travels from the transmitter side and back to the receiver after hitting a distant target. Owing to the presence of reflecting walls in TWRI applications, the multipath spread of EM waves introduces false time delays. Consequently, the receiver declares the presence of targets that do not physically exist in the actual scene. These hypothetical targets are called ghosts [1]–[3]. The number of ghosts expected in a reconstructed image is dictated by the number of registered multipath returns. Since the number of multipath returns in TWRI is higher than the number of direct returns, the formed ghosts outnumber the genuine targets; therefore, target detection and recognition will be highly vulnerable. Without an effective and efficient ghost suppression mechanism, TWRI technology may incorrectly interpret the scene, which can lead to improper resource allocation.

The current trend in TWRI applications is to obtain highly resolved images, as in [1]–[3]. The image resolution along the crossrange and downrange requires a large aperture and wide bandwidth, respectively. Consequently, a large amount of data needs be collected and processed. This explains why, in modern TWRI, the application of compressive sensing (CS) found considerable attention. CS techniques enable us to acquire and reconstruct a sparse signal using a small fraction of linear projections of the original signal without compromising the signal quality [4]. The vector is reconstructed by sparse reconstruction techniques such as minimization of the ℓ_1-norm using a number of algorithms

including basis pursuit, matching pursuit (MP) and its derivatives [5], and Bayesian matching pursuit with or without a Gaussian input [6]. The minimum required number of measurements is usually much smaller than the length of the signal but nearly proportional to the number of nonzero entries. In TWRI, this optimal number of measurements is highly sensitive to the presence of ghost targets. This problem severely affects the performance of CS algorithms but has not been rigorously addressed yet in the literature. Most of the available ghost suppression techniques under the CS framework aim to increase the probability of correct target detection.

This article presents a fairly thorough study of multipath ghosts in TWRI applications. Different ghost suppression methods are reviewed: with/without multipath exploitation and under the CS framework or full data volume. Their strengths and weaknesses are presented, paving the way for further research.

The paper is organized as follows. Section II describes the TWRI scene model. Ghost formation is described in Section III. Section IV and V respectively summarize the challenges and properties of ghosts. Suppression techniques are delineated in Section VI, and a performance comparison is presented in Section VII. Finally, Section VIII presents the conclusions.

II. TWRI Scene and Signal Models

Consider a scene of an indoor rectangular room as a typical scenario of TWRI application. The top view of the scene, shown in Fig. 1, comprises front, back, and side walls with a thickness of d_i and relative permittivity ε_i. An antenna array or a synthetic aperture radar (SAR) with N specified radar locations is located parallel to the front wall at a distance d_f.

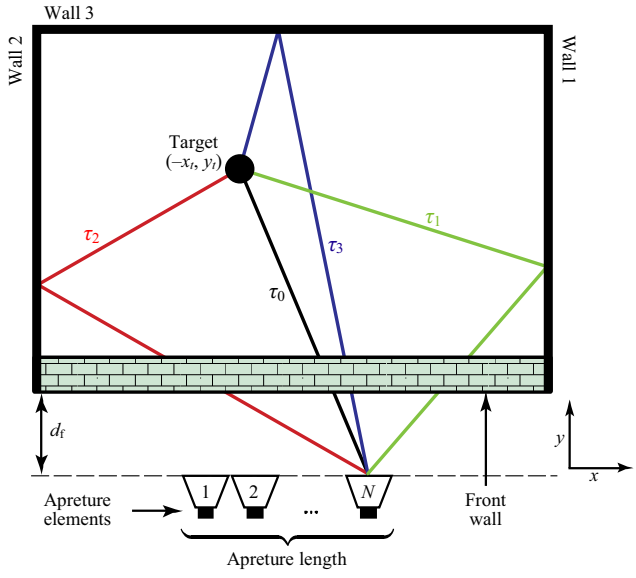

Fig. 1. TWRI scene model with first-order returns.

In the TWRI literature, the scene of interest is interrogated using either pulsed radar or a stepped-frequency radar system. In these two scenarios, the transmitted ultrawideband (UWB) signal is realized in the time and frequency domains, respectively. To acquire a higher resolution with pulsed radar, the transmitted pulses should have a shorter time duration, thereby increasing the transmitted bandwidth [7], [8]. As presented in the radar literature, the signal-to-noise ratio (SNR) depends on the transmitted energy of the radar signal [9]. The energy of a pulse is specified by the transmitted peak power in the pulse and the pulse width. When transmitting shorter pulses to achieve a higher range resolution, a low energy is transmitted; hence, the SNR is reduced for a given transmitter power. Radar engineers have suggested radar waveforms with a longer time to acquire a high energy but at the same time give a better range resolution. One approach is to transmit a series of M monochromatic waves of linearly increasing frequency one after the other, known as a stepped-frequency signal [7], [8].

To reach behind-the-wall targets, the signal is refracted at the air–wall interface and then at the wall–air interface, and the backscattered signal follows the reverse path to the receiver. This round trip, which is mainly caused by target reflection, is referred to as *direct return*.

Owing to the presence of interior and front walls, some of the signal components are reflected by these secondary scatters once or more before reaching the receiver. These signal components involving the targets and surrounding walls or the interaction between the targets themselves are referred to as *multipath returns*. A multipath return that results from a single bounce is termed a *first-order* return. Otherwise, it is *second-order* or *higher-order* if it undergoes two or more bounces, respectively. In TWRI, only a few orders are significant, as higher-order returns suffer from either cumulative attenuation when striking the walls or a prolonged round-trip delay, making their effect very weak or residing outside the given scene [2].

The presence of a floor and ceiling gives another type of multipath return, which accounts for the ghosts in three-dimensional (3D) imaging when considered in the signal model. Moreover, we expect a multipath return due to the target-to-target interaction. The ghost formation due to target interactions will not be dealt in this paper.

Another type of multipath return results from multiple reflections within the front wall as the signal travels to the target or back to the receiver after the target interaction, as

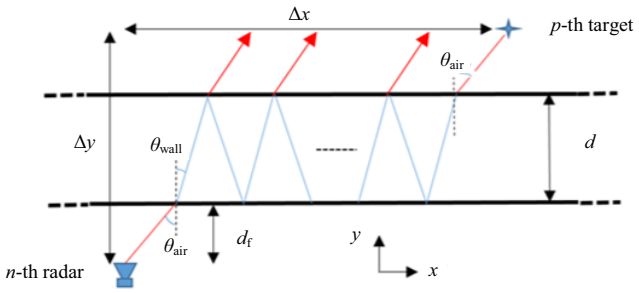

Fig. 2. Front-wall reverberation model [2].

shown in Fig. 2. This phenomenon is called *wall ringing* or *reverberation*.

The horizontal distance between the target and the array element, Δx, in Fig. 2, can be expressed as

$$\Delta x = d_{\mathrm{f}} \tan\theta_{\mathrm{air}} + d(1+2k)\tan\theta_{\mathrm{wall}} + (\Delta y - d - d_{\mathrm{f}})\tan\theta_{\mathrm{air}},$$

$$\Delta x = (\Delta y - d)\tan\theta_{\mathrm{air}} + d(1+2k)\tan\theta_{\mathrm{wall}}, \qquad (1)$$

where Δy is the distance between the target and the array element in the downrange direction; θ_{air} and θ_{wall} are the angles in air and in the wall medium, respectively; d_{f} is the standoff distance, and k is the number of wall reverberations. The angles θ_{air} and θ_{wall} are related by Snell's law as

$$\frac{\sin\theta_{\mathrm{air}}}{\sin\theta_{\mathrm{wall}}} = \sqrt{\varepsilon_{\mathrm{r}}}, \qquad (2)$$

where ε_{r} represents the relative permittivity of the front wall.

The one-way time delay that a given return will undergo owing to k wall reverberations will be [3]

$$\tau(\Delta x, \Delta y, k) = \frac{(\Delta y - d)}{c\cos\theta_{\mathrm{air}}} + \frac{d\sqrt{\varepsilon_{\mathrm{r}}}(1+2k)}{c\cos\theta_{\mathrm{wall}}}, \qquad (3)$$

where c is the speed of an EM wave in free space. Since the magnitude of the signal is attenuated when it is reflected within the wall, only a few reverberations will be noticeable.

In the literature, received signal models are either presented in the time or frequency domain. In time-domain TWRI, the signal received at the nth receiver is a superposition of all echoes of the transmitted pulse [10]:

$$y_n(t) = \sum_{r=0}^{R} \sum_{p=0}^{N_x N_y - 1} \sigma_p s(t - t_{np}^{r}). \qquad (4)$$

The received signal at nth location when the mth frequency f_m is transmitted for R multipath returns comprises four main contributions: reflection from the front wall, target-to-side wall reflection, target-to-target reflection, and ambient noise, as given in [11], [12] by

$$\begin{aligned} y[m,n] = &\sum_{r=0}^{R-1} \sum_{p=0}^{N_x N_y - 1} \sigma_p^{(r)} \exp\left(-j2\pi f_m t_{pn}^{(r)}\right) \\ &+ \sum_{r_{\mathrm{w}}=0}^{R_{\mathrm{w}}-1} \sigma_{\mathrm{w}}^{(r_{\mathrm{w}})} \exp\left(-j2\pi f_m t_{\mathrm{w}}^{(r_{\mathrm{w}})}\right) \\ &+ \sum_{r=0}^{R-1} \sum_{p,q=0 p\neq q}^{N_x N_y - 1} \sigma_{pq}^{(r)} \exp\left(-j2\pi f_m t_{pqn}^{(r)}\right) \\ &+ v(m,n), \end{aligned} \qquad (5)$$

where $t_{pn}^{(r)}$ represents the round-trip delay between the pth target and the nth receiver due to the rth return, $t_{pnq}^{(r)}$ is the round-trip delay between the pth and qth targets with the nth transceiver, and $t_{\mathrm{w}}^{(r_{\mathrm{w}})}$ is the time delay of the $r_{\mathrm{w}}^{\mathrm{th}}$ front wall return. Moreover, $\sigma_p^{(r)}$ and $\sigma_{\mathrm{w}}^{r_{\mathrm{w}}}$ are the target and wall pixel reflectivities, respectively, with respect to the rth return, and $v(m,n)$ is the noise sample.

Since the contributions from the target interactions in (5) is nonlinear, it was suggested in [11] that the overall signal reflectivity due to the target interactions, $\sigma_{pq}^{(r)}$, is dictated by the second target, and the first target was taken as a perfect reflector.

In conventional SAR imaging, only the direct return gives the correct target location, and the remaining $R-1$ returns result in ghost targets if not handled properly.

III. Ghost Formation in TWRI

In TWRI applications employing SAR, ghost targets result from the interaction of genuine targets or targets with secondary reflectors. The front wall causes a ghost only when the signal component undergoes multiple internal reflections. The ghosts due to the front-wall reverberation effect appear in the downrange direction, and their spacing is a function of the wall properties as elaborated in [2], [3]. When a signal travels from the transceiver to the target, part of it propagates straight to the target, and the other components are reflected by the walls, floor, and ceiling before reaching the target or after being reflected. The signal components scattered by the same target register different delays due to different reflecting geometries, as shown in Figs. 3(a) to 3(c). Fig. 3(a) shows direct propagation; in Fig. 3(b), the signal is reflected once by the side wall only as it traverses to the receiver. Fig. 3(c) shows second-order reflection, which involves a double bounce via the side wall. In such scenarios, the receiver interprets each of the delayed versions as they come from different physical targets and results in hypothetical targets, as depicted in Fig. 3(d). The formed ghosts with the true target fall on concentric

https://doi.org/10.4218/etrij.2017-0241

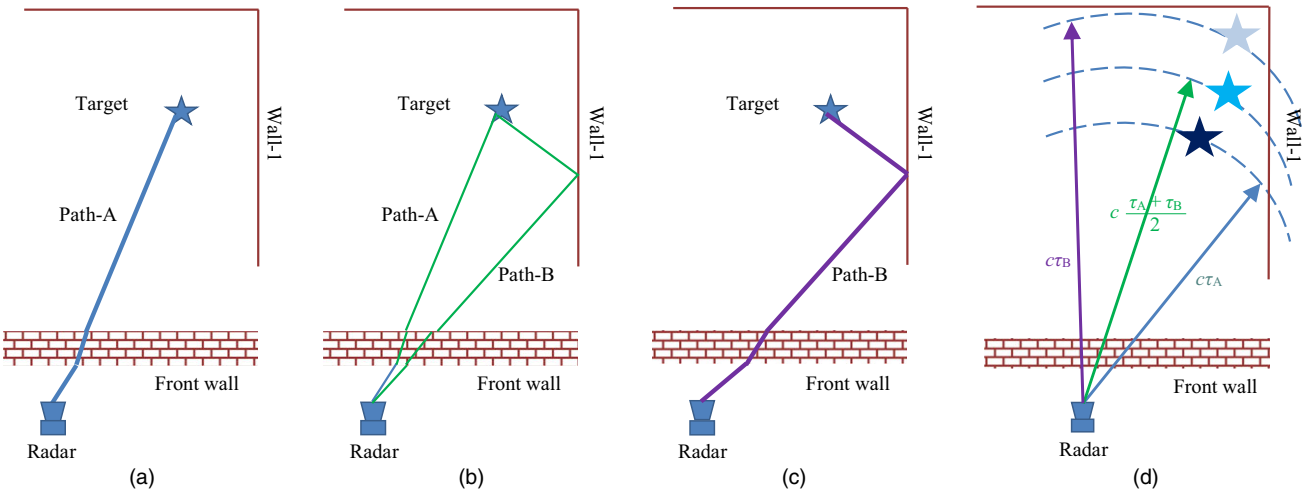

Fig. 3. Some indoor multipath scenarios: (a) direct return, (b) first-order multipath return, (c) second-order multipath return, and (d) the corresponding target and ghost locations.

circles with the transceiver location being their common center. In this way, the scene becomes populated, and the number of expected ghosts grows in proportion to the number of true targets for a given reflecting geometry. Suppose that there are P true targets in the scene and R signal returns from every target were recorded by the transceiver. The number of multipath ghosts is upper-bounded by $P(R-1)$.

Consider a monostatic configuration; the locus of the ghost location with respect to the transceiver and a given wall can be calculated. Referencing Figs. 3(a) to 3(c), suppose that the time delay of the signal travels from the radar to the target through Path-A is τ_A and that from the target to the radar through Path-B is τ_B. The possible location of the true target is described by the circle with a radius of $c\tau_A$, where c denotes the speed of light in free space. The locus of the ghost location due to a single bounce (first-order reflection) on the right-side wall is a circle with a radius of $c\left(\frac{\tau_A+\tau_B}{2}\right)$, as shown in Fig. 3(d). If the signal undergoes reflection twice at the wall (second-order reflection), the resulting ghost will reside $c\tau_B$ away from the radar, as depicted in Fig. 3(d) with $\tau_B > \left(\frac{\tau_A+\tau_B}{2}\right) > \tau_A$. The presence of the left and back walls generates ghosts in the given scene in a similar fashion. During SAR image reconstruction and interpretation, the formed ghost targets pose some technical challenges, as will be highlighted in the next section.

IV. Challenges Related to Ghosts in TWRI

In TWRI, multipath ghosts present two technical challenges: confusion with the genuine target and a degradation in the performance of CS algorithms. When reconstructing the SAR image in the presence of multipath ghosts, it is difficult to correctly detect the target in such a scenario. If second- and higher-order returns are considered and/or the number of targets increases, then the probability of correct target detection is reduced drastically. This effect has been articulated in the literature well, and different techniques have been devised to mitigate or eliminate this effect [2], [3], [7], [8], [13]–[16].

Recently, the application of CS has revolutionized the field. However, ghosts render the scene sparsity and therefore degrade the performance of CS algorithms. To utilize the technology at its best, this performance degradation needs to be investigated.

In the CS literature, the number of random measurements in a nonmultipath scenario, J_1, which is required to reconstruct a sparse vector of length N_xN_y, is given by

$$J_1 \geq CP\log\left(\frac{N_xN_y}{P}\right), \tag{6}$$

where C is a small constant.

If there are P genuine targets in a room and R total returns have been registered, the image vector in TWRI will contain up to PR targets (genuine and ghosts); hence, the sparsity sense may be violated, and the minimum required number of measurements will be inadequate. As an example, Fig. 4(a) shows a sketch of a room with two targets to be imaged. The conventional SAR image is shown in Fig. 4(b). The two targets are surrounded by green circles, while ghosts are indicated by the blue polygons. In this case, the suitable number of random measurements required to reconstruct the vector, J_2 will be

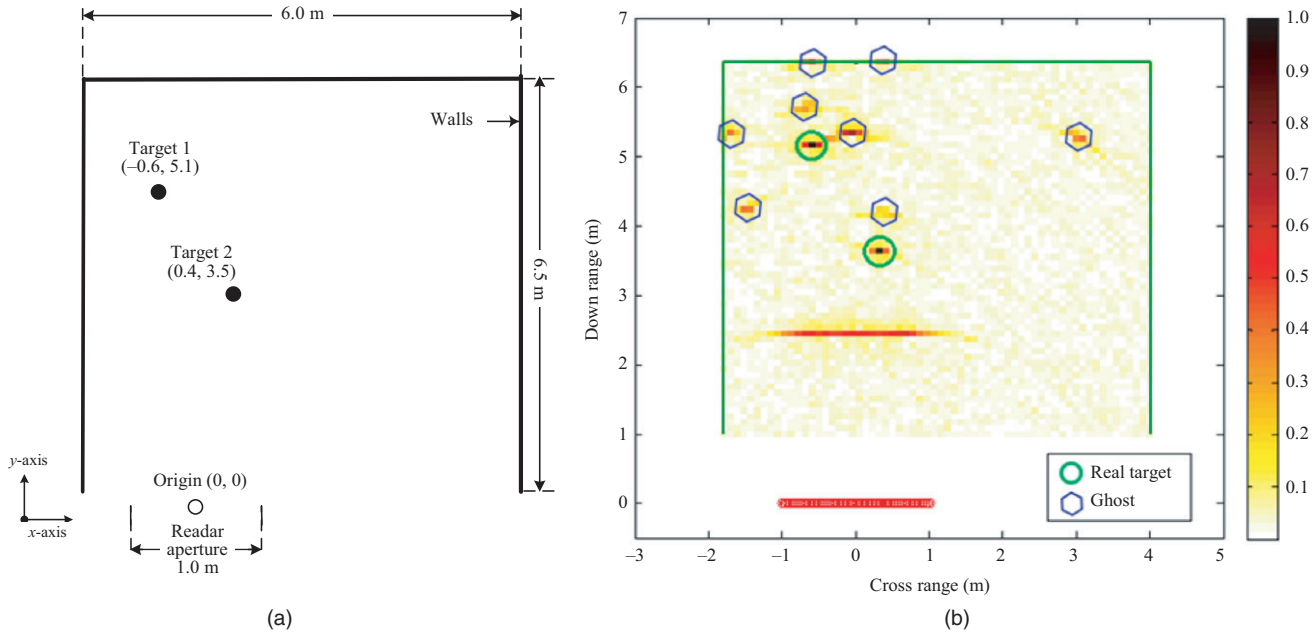

Fig. 4. (a) Sketch of a scene comprising two targets. (b) Conventional radar image of (a); multipath ghosts are enclosed with polygons.

$$J_2 \geq CPR \log\left(\frac{N_x N_y}{PR}\right). \quad (7)$$

To reconstruct TWRI in a multipath scenario, extra measurements are needed to reconstruct the same number of targets compared to the outdoor case. This problem limits the allowable number of indoor targets for perfect reconstruction. Thus far, the effect of the number of targets due to the presence of ghosts on the performance of CS has not been extensively analyzed, and most available studies in the literature perform post image processing to suppress ghosts.

To tackle this challenge, preprocessing the received data is needed to reduce the effect of ghosts before applying image reconstruction algorithms. A received signal model should be suggested to ensure ghost-free image reconstruction to better utilize CS capabilities. Detailed information regarding CS and its application to TWRI can be obtained in [17].

V. Properties of Multipath Ghosts

Among the properties of ghosts is the lower crossrange resolution, nonideal focusing, and aspect dependence (AD).

1. Lower Crossrange Resolution

In SAR imaging, the downrange resolution and crossrange resolution of a point target are functions of the signal bandwidth and aperture size, respectively. During through-the-wall sensing, a direct return is registered at every radar location, making the image of the true target highly resolved in the crossrange direction. However, multipath returns only exist at some locations in SAR, making the image of the ghost target exhibit less resolution compared to that of the real target. This explains why the ghosts exhibit a *lower crossrange resolution*.

2. Nonideal Focusing

Multipath propagation not only results in a ghost at a given point but also disturbs the focus line owing to the change in the signal phase. Consequently, the ghosts deviate the prospective focusing location. This characteristic of a ghost is referred to as *nonideal focusing.*

3. Aspect Dependence

In TWRI, a change in the transceiver location alters the signal reflection pattern and therefore registers different round-trip delays. If the scene is interrogated using different apertures, their corresponding ghosts reside at different pixels. This property is referred to as the *aspect dependence*. On the other hand, the true targets maintain the same pixels regardless of the changes in the radar locations, making the identification of a ghost from a

https://doi.org/10.4218/etrij.2017-0241

genuine target possible. The effectiveness of this property on ghost suppression is demonstrated in [2], [3], [14], [18].

VI. Multipath Exploitation and Ghost Suppression Techniques

In the TWRI literature, different techniques have been presented to eliminate the effects of multipath ghosts with the aim of improving the probability of accurate target detection or enhancing the quality of the image. Broadly, we can categorize multipath treatment techniques into three groups: multipath-exploitation-based techniques [7], [8]; AD-based techniques [13], [14], [16], [18], [19]; and CS-based approaches [20]. Recent contributions integrate multipath exploitation with CS to reconstruct a ghost-free image [21], [22]. Moreover, there is an emerging interest in the exploitation of the AD characteristics under the CS frame, as presented in [2].

This section presents the current multipath exploitation and ghost suppression techniques available in the literature. Their pros and cons are enumerated, and future extensions are suggested for healthy contributions.

1. Multipath-Exploitation-Based Ghost Suppression

There are two common cases regarding multipath exploitation in the literature: exploitation under the resolved multipath assumption [2], [7], [21], [22] and unresolved multipath cases [23]–[26]. With the application of UWB signals, the former assumption is justifiable, and that will be our focus.

In [7], multipath exploitation was utilized, assuming stationary or slowly moving point targets. The proposed technique starts by forming an SAR image, then determining the locations of the ghosts for each target, and mapping each ghost back onto its corresponding target location, which increases the signal-to-clutter ratio (SCR) at the genuine target locations.

Consider Fig. 5, where the right wall is located at $(w_1, 0)$, and the nth radar is located at $(-D_n, 0)$ with the origin defined at the center of the array, as in [7]. Suppose that the ghost due to Wall-1 is located at (x_{n_1}, y_{n_1}). When the signal is reflected from the wall from the target, it creates a virtual radar location, as shown in Fig. 5, and forms a bistatic configuration. The locations of the ghosts caused by a single bounce from the right wall as viewed by the nth radar is the intersection of the monostatic locus, which is the circle with a radius of $\tau = c\left(\frac{\tau_A+\tau_B}{2}\right)$ centered at $(D_{n1}, 0)$, and bistatic locus, which is the ellipse with foci at the real and virtual radar locations, as depicted in Fig. 5. The equations describing the two loci are

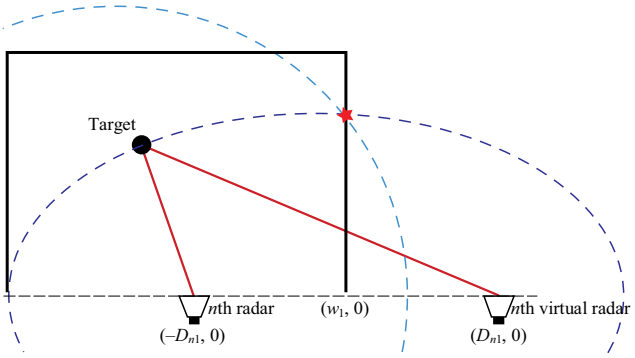

Fig. 5. Ghost location due to the right wall.

$$(x_{n_1} - D_{n_1})^2 + y_{n_1}^2 = c^2\tau^2, \tag{8}$$

$$\frac{4(x_{n1} - w_1)^2}{c^2\tau^2} + \frac{4y_{n_1}^2}{c^2\tau^2 - D_{n_1}^2} = 1. \tag{9}$$

Solving (5) and (6), $x_{n_1} = w_1$, and its corresponding y_{n_1} is given by

$$y_{n_1} = \pm\sqrt{\frac{c^2\tau^2}{4} - (w_1 - D_{n_1})^2}. \tag{10}$$

The focused ghost location due to the right wall can be determined using a least-squares method for all locations. A similar procedure is adopted to locate the ghosts associated with the rest of the walls.

Knowing the location of the multipath ghost associated with each pixel, the energy of the associated ghosts is mapped back onto the genuine target's location forming an *intermediate image*. This is achieved by two-dimensional (2D) weighting functions that use the information of the ghost locations [7].

The function is chosen such that the full energy of the ghosts is utilized to boost the amplitude of the real target while suppressing the ghosts; see [7] for details. Finally, a composite ghost-free image is obtained by pixel-wise multiplication of the initial and intermediate images.

The technique involves complex mathematical expressions, especially when the front wall is taken into account. It requires complete knowledge of the reflecting geometry, which is not always obtainable. Moreover, when the ghost overlaps with a true target location, which is possible if the number of targets increases, the technique will underperform. The technique does not account for the ghosts due front-wall reverberation as well.

2. Multipath Exploitation with Sparse-Reconstruction-Based Ghost Suppression

Leigsnering and others in [3] proposed an image reconstruction technique using the group sparsity with multipath exploitation. They incorporated the front-wall reverberation effect, which makes their approach more practical. The received signal model groups all returns from the same wall into one measurement matrix. During the image reconstruction process, the method inverts the multipath model assuming prior knowledge of the reflecting geometry.

Suppose that there are N radar locations for the scene interrogation shown in Fig. 1. At each location, M equally spaced monochromatic waves are transmitted and received to realize a UWB signal. If we have N_x and N_y pixels along the crossrange and downrange, respectively, the target reflectivity of the pth pixel is represented by σ_p, with $p = 0, 1, \ldots, N_xN_y - 1$. If there are R total returns, then the received signal at the nth radar position when the mth frequency f_m is transmitted is given by (5) and its corresponding vector representation [3]:

$$\mathbf{y} = \mathbf{\Phi}^{(0)}\mathbf{s}^{(0)} + \mathbf{\Phi}^{(1)}\mathbf{s}^{(1)} + \ldots + \mathbf{\Phi}^{(R-1)}\mathbf{s}^{(R-1)} + \mathbf{v}, \quad (11)$$

where $\mathbf{s}^{(r)} \in \mathbb{C}^{N_xN_y \times 1}$, $r = 0, 1, \ldots, R - 1$ represents the vectors of the reflectivities $\sigma_p^{(r)}$. For simplicity, the weights of the returns are included in $\sigma_p^{(r)}$, $\mathbf{v} \sim G(0, \sigma^2\mathbf{I})$, and $\mathbf{\Phi}^{(r)} \in \mathbb{C}^{MN \times N_xN_y}$ is the dictionary matrix containing the phase information of the target due to the rth return with entries defined as

$$[\mathbf{\Phi}^{(r)}]_{ip} = \exp(-j2\pi f_m t_{pn}^{(r)}), \quad (12)$$
$$m = i \bmod M, n = \left\lfloor \frac{i}{M} \right\rfloor,$$
$$i = 0, 1, 2, \ldots, MN - 1.$$

To apply CS, (11) is multiplied by the downsampling matrix $\mathbf{D} \in \{0, 1\}^{J \times MN}$ with $J \ll MN$. Basically, $\mathbf{D}$ is a Bernoulli matrix that is obtained by randomly selecting J rows from an $MN \times MN$ identity matrix. Downsampling (11) gives

$$\bar{\mathbf{y}} = \mathbf{A}^{(0)}\mathbf{s}^{(0)} + \mathbf{A}^{(1)}\mathbf{s}^{(1)} + \ldots + \mathbf{A}^{(R-1)}\mathbf{s}^{(R-1)} + \bar{\mathbf{v}} \quad (13)$$

with $\mathbf{A}^{(r)} = \mathbf{D}\mathbf{\Phi}^{(r)}$. The above equation can be rewritten as the product of a fat matrix of dictionaries and a tall vector stacking all subimages:

$$\bar{\mathbf{y}} = \mathbf{B}\mathbf{s} + \bar{\mathbf{v}},$$

$$\mathbf{B} = [\mathbf{A}^{(0)}\mathbf{A}^{(1)} \ldots \mathbf{A}^{(R-1)}] \in \mathbb{C}^{J \times N_xN_yR},$$

$$\mathbf{s} = [(\mathbf{s}^{(0)^T})(\mathbf{s}^{(1)^T}) \ldots (\mathbf{s}^{(R-1)^T})]^T. \quad (14)$$

To reconstruct the unknown reflectivity vectors, $\mathbf{s}$, using the compressed measurements, $\bar{\mathbf{y}}$, a group sparse reconstruction using mixed ℓ_1 - ℓ_2 norm regularization can be used [3]:

$$\tilde{\mathbf{s}} = \arg\min_s \|\bar{\mathbf{y}} - \mathbf{B}\mathbf{s}\|_1 + \gamma\|\mathbf{s}\|_{2,1},$$

$$\|\mathbf{s}\|_{2,1} = \sum_{p=0}^{N_xN_y-1} \sqrt{\sum_{r=0}^{R-1} s_p^{(r)} \left(s_p^{(r)}\right)^*}, \quad (15)$$

where γ is a regularization parameter. Solving the mixed norm problem in (15) and combining the subimages to obtain the final image, $\mathbf{s}_\mathrm{f}$ is obtained by forming the Euclidean norm over each group [3]:

$$[\mathbf{s}_\mathrm{f}]_p = \left\| \left[s_p^{(0)}, s_p^{(1)}, \ldots, s_p^{(R-1)} \right]^T \right\|_2. \quad (16)$$

A similar experimental setup and measurement volume were adopted to generate the results, as in [3].

Fig. 6(a) shows image reconstruction using conventional CS, and Fig. 6(b) shows the image reconstructed using the group sparse reconstruction presented in [3].

This technique faces the following challenges; it requires complete knowledge of the geometry, which is not always available. It requires large matrices, resulting in a high memory demand and prolonged processing time. Moreover, it does not account for ghosts due to the interactions between targets.

The authors in [22] also proposed a CS-based multipath ghost suppression technique using SAR assuming prior knowledge of the geometry. On the basis of a multipath model, an overcomplete dictionary that accounts for interactions between the radar, targets, and environment was constructed.

There is a contribution in sparsity-based scene reconstruction with multipath suppression instead of exploitation presented by [20]. The authors proposed a received signal model, $y(t, n)$, at the nth radar location in a multipath environment as the sum of the direct impulse response and multipath impulse response for P targets convolved with the transmitted pulse waveform $s(t)$ as

$$y(t, n) = \sum_{p=1}^{P} s(t) * \left(g_p(t, n) + d_p(t) * g_p(t, n)\right), \quad (17)$$

where $g_p(t, n)$ is the direct impulse response, which is taken to be a single spike and stronger than the indirect

https://doi.org/10.4218/etrij.2017-0241

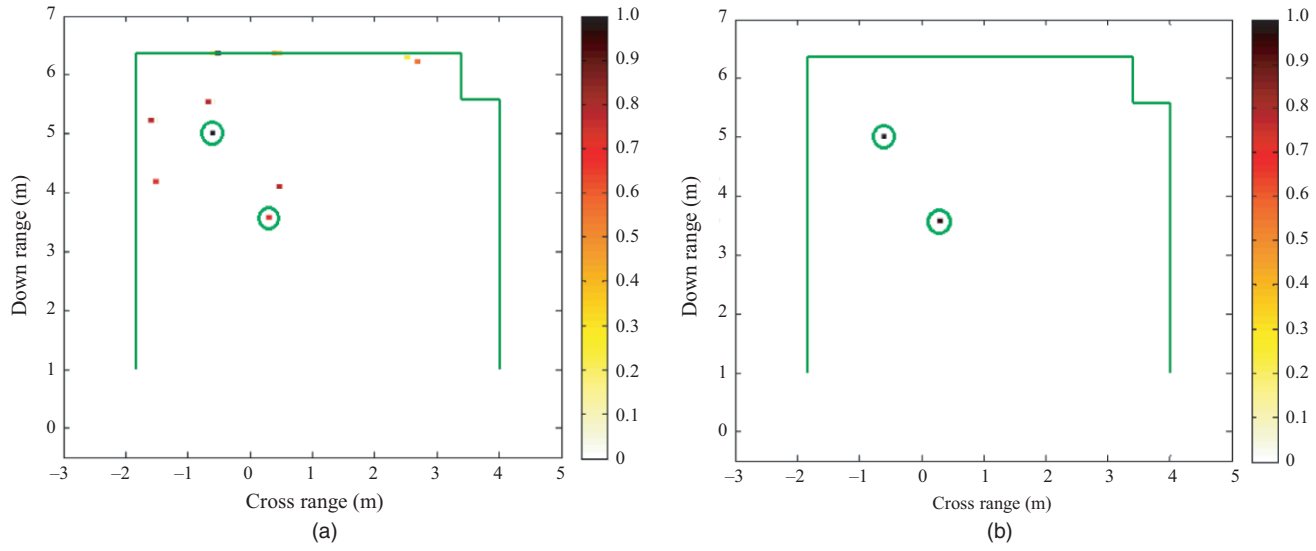

Fig. 6. Simulation results: (a) conventional CS and (b) group sparse CS.

returns. On the other hand, the multipath impulse response is defined as the convolution of the direct impulse response $g_p(t,n)$ and a sparse delay function $d_p(t)$. The multipath delays for a particular target are assumed to be constant across the receivers. The authors iteratively estimate the primary impulse response and sparse delay using a sparse reconstruction approach. The primary impulse response is then used to generate a ghost-free image. The attractive feature of this approach is its independence of the reflecting geometry. However, it suffers from error propagation and complexity as a result of repeated convolutions.

3. Aspect-Dependence-Based Ghost Suppression

There are contributions utilizing the AD feature of multipath ghosts. The authors of [13] proposed a ghost suppression technique utilizing the AD feature of ghosts. The authors observed the variations in the intensities of the image pixels of L subaperture images by evaluating the normalized standard deviation I_{NSTD} [13]:

$$I_{\mathrm{NSTD}}(x,y) = \frac{\sqrt{\sum_{l}^{L}\left[I_l(x,y) - \bar{I}_l(x,y)\right]^2}}{L \cdot \bar{I}_l(x,y)}, \qquad (18)$$

$$\bar{I}_l(x,y) = \frac{\sum_{l}^{L} I_l(x,y)}{L}$$

where $I_l(x,y)$ is the intensity of pixel (x,y) in lth subaperture image. By subaperture, we mean that a subset of the available radar locations is utilized during image formation. A pixel with a high deviation value is announced as a ghost target and is therefore suppressed or attenuated; otherwise, it is retained. In this way, a ghost-free image is generated.

In [14], [18], the authors proposed a multipath ghost suppression method for target–target interactions by observing the variations in the intensities of the target and ghost pixels. Since the target intensity depends on its orientation, which is unknown, the authors modeled the variation in the target intensity across various subaperture images as a hidden Markov model (HMM).

This method requires training data from known targets to estimate the state-transition and initial state probabilities. During training, subaperture images are generated from the full aperture image using directional filters. If the pth image pixel has an intensity profile I_p, the trained HMM is used to evaluate the likelihood probability that the observed intensity profile is generated by the given target. The likelihood is given by

$$P(I_p|P_1) = \sum_{\text{all } q} P(I_p|q,P_1)P(q|P_1), \qquad (19)$$

where $P(I_p|q,P_1)$ is the probability that I_p was generated by state sequence q given the target P_1, and $P(q|P_1)$ is the probability that the state sequence q occurs given the target P_1.

The output of the pixel value, $y(i,j)$, after the pixel mask for the given (i,j) pixel value, $s(i,j)$, is

$$y(i,j) = P(I_p|P_1)s(i,j). \qquad (20)$$

However, their method requires image decomposition into N subaperture images using directional filters and also requires complex advanced algorithms with training phases, which make the method relatively complex.

In [16], the authors proposed a multipath ghost suppression technique exploiting the AD feature using marginal subapertures. To generate results, they adopted nearly the same setup and measurement volumes as in [16]. Three images are generated: one using the whole aperture (Fig. 7(a)), $I(i, j)$, and two using subapertures from the two extreme ends of the room denoted by $I_1(i, j)$ and $I_2(i, j)$ (Fig. 7(b) and Fig. 7(c) respectively).

The left and right subapertures are selected such that the multipath echoes reflected by the right and left walls, respectively, are avoided. The final image $I_f(x,y)$ shown in Fig. 7 is the product of the three images:

$$I_f(x,y) = I(x,y) \times I_1(x,y) \times I_2(x,y). \quad (21)$$

The method involves the tedious searching of appropriate subapertures and the shifting of the antenna array to two extreme ends of the room, which increases the complexity and processing time. It also suffers from remnants, which demand post image processing. However, the attractive feature of this method is the simplicity of obtaining the final image.

In [25], the authors proposed a suppression technique for ghosts originating from only target-to-target interactions based on subarray imaging. They suggested different array configurations with image combining strategies to combat the effects of multipath ghosts, taking into account the AD feature of the multipath ghosts. However, the effects of the side walls when considering TWRI are significant and cannot be left out.

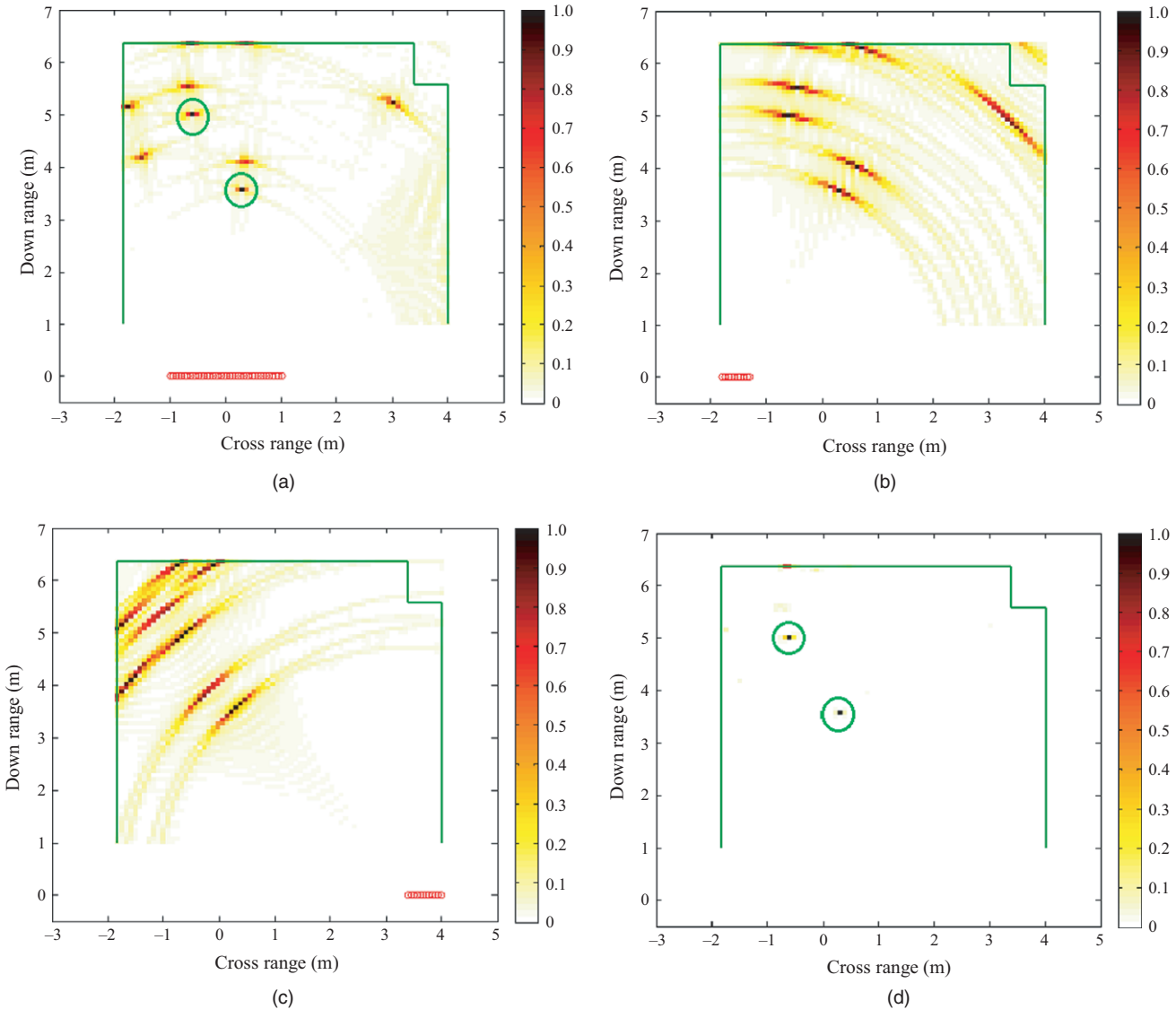

Fig. 7. Ghost suppression: (a) full aperture image, (b) Subaperture-1, (c) Subaperture-2, and (d) final image.

https://doi.org/10.4218/etrij.2017-0241

4. Aspect Dependence with Sparse-Reconstruction-Based Ghost Suppression

In this category, there are two regimes: realizing AD by using subapertures with random radar locations [2] and by using sparse arrays. In this case, a Pythagorean aperture under sparse reconstruction was devised in [27].

A. Random Subapertures with Sparse Reconstruction

Following the application of CS in TWRI, the multipath ghost suppression methods based on the AD feature of ghosts discussed above cannot be adopted as they are. The minimum required number of measurements and the modality need to be observed in order to correctly reconstruct the sparse image. To address these challenges, the authors of [2] proposed a multipath ghost suppression technique that incorporates the AD feature of multipath ghosts under the CS framework. They reconstructed images using multiple measurement vectors with only direct path information, which reduces the complexity significantly. Multiple measurements are selected such that the AD feature in the resulting images is pronounced. Instead of using the reverse model, as in [3], they relaxed the model to

$$\mathbf{y} = \mathbf{\Phi}^{(0)}\check{\mathbf{s}}^{(0)} + \mathbf{v}, \tag{22}$$

where $\check{\mathbf{s}}^{(0)}$ is the modified image containing the contributions from multipath returns.

Then, independent sets of measurements are acquired using undersampling matrices $\mathbf{D}_i \in \{0,1\}^{J\times MN}, i = 1,2$ with $J \ll MN$. Downsampling the given observation gives

$$\bar{\mathbf{y}}_i = \mathbf{D}_i\mathbf{\Phi}^{(0)}\check{\mathbf{s}}_i^{(0)} + \bar{\mathbf{v}}_i. \tag{23}$$

$\mathbf{D}_i$ is selected such that the ghost locations in the corresponding images exhibit significant differences and can therefore be identified and suppressed. It is shown in [2] that randomly selecting measurements in the first half of the given array and the second set of measurements as the corresponding locations of the first yields the best performance.

With a high probability, the reconstructed vector $\tilde{\check{\mathbf{s}}}^{(0)}$ is obtained by the solving optimization problem

$$\tilde{\check{\mathbf{s}}}_l^{(0)} = \arg\min_{\check{\mathbf{s}}_i^{(0)}} \left\|\check{\mathbf{s}}_i^{(0)}\right\|_1 \text{ s.t. } \left\|\bar{\mathbf{y}}_i - \mathbf{A}_i\check{\mathbf{s}}_i^{(0)}\right\|_2 < \varepsilon \tag{24}$$

with $\mathbf{A}_i = \mathbf{D}_i\mathbf{\Phi}^{(0)}$. The choice of ε is a function of the noise power given by

$$\varepsilon = \sigma\sqrt{2\log\left(N_x \times N_y\right)}, \tag{25}$$

where σ is the standard deviation of the noise. Figs. 8(a) and 8(b) show the images reconstructed using the first and second measurement sets, and Fig. 8(c) is the final image. The final image in Fig. 8(c) is obtained by the multiplicative fusion of the individual images or evaluating the group normalized variance. This scheme does not account for the target-to-target interaction, which is expected in TWRI scenarios.

B. Pythagorean Apertures with Sparse Reconstruction

Unlike in the random subaperture radar selection scenario, the measurement matrix in this case is designed using predefined radar locations, as in [27].

In [27], the authors proposed sparse arrays based on a Pythagorean triple. Three array configurations were examined: a Pythagorean-based interlaced subarray (PISA), a Pythagorean-based displaced subarray (PDSA), and a spatial orthogonal coprime array (SOCA).

In a PISA, two Pythagorean coprime triple arrays are amalgamated to form a long array such that the radar location, say x, is defined as $\boldsymbol{x} = [x_1, x_2, \ldots, x_{|S_1 \cup S_2|}]^T$,

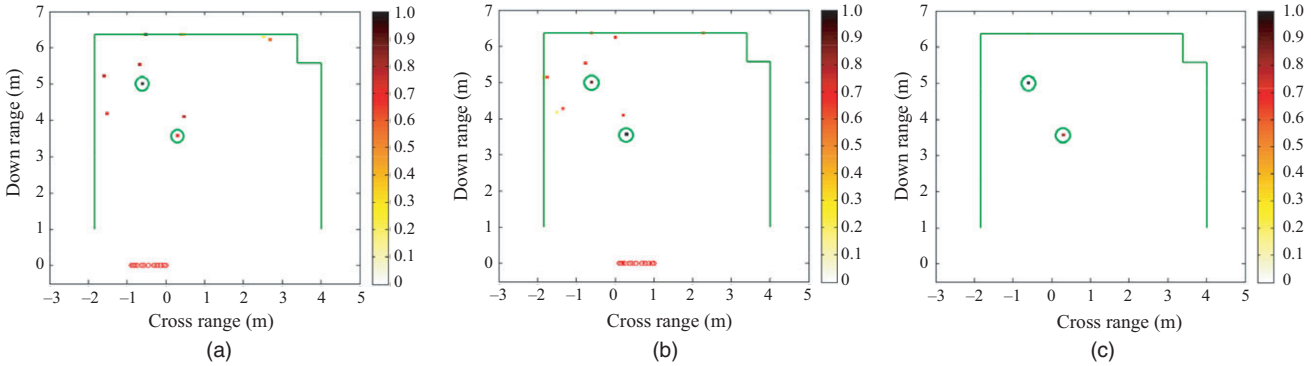

Fig. 8. Ghost suppression: (a) Subaperture-1, (b) Subaperture-2, and (c) final image.

where $x_i \in S_1 \cup S_2$, $i = 1, \ldots, |S_1 \cup S_2|$, and S_1 and S_2 are the Pythagorean coprime subapertures defined in [27].

In a PDSA, before merging S_1 and S_2, S_2 is displaced such that it is separated from S_1 by a distance L, where L is the minimum of two lengths. The radar location x is chosen from $\boldsymbol{x} = [x_1, x_2, \ldots, x_{|S_1 \cup \tilde{S}_2|}]^T$, where $x_i \in S_1 \cup \tilde{S}_2$, $i = 1, \ldots, |S_1 \cup \tilde{S}_2|$ [27].

In an SOCA, the Pythagorean triple subarrays are mutually perpendicular. The configuration is affected by the standoff distance and front-wall mitigation; therefore, it has limited applications. The radar location (x, y) is a vector defined by $\mathbf{x} = [x_1, x_2, \ldots, x_{|S_1|}]^T$ and $\mathbf{y} = [y_1, y_2, \ldots, y_{|S_2|}]^T$ from the horizontal and vertical subarrays, respectively [27].

A setup similar to that in [27] was adopted to reproduce the results. The left and right sidewalls of the room reside at the crossranges of –3 m and 3 m, respectively, and the back wall is at a downrange of 6 m. A front wall with a thickness of 20 cm and a relative permittivity $\varepsilon_r = 7.67$ is at a standoff of 2 m. A series of 201 monochromatic waves occupying a spectrum between 1 GHz and 3 GHz was used to interrogate the scene. An array of 4 m with an interelement spacing of 0.019 m was used to interrogate the scene. The lengths of the Pythagorean subarrays are similar to those in [27]. Two metallic cylinders with a diameter of 0.2 m and a length of 0.6 m are used as targets located at (−0.5,4) m and (1.5,4) m.

The images using the PISA, PDSA, and SOCA are depicted in Fig. 9(a), 9(b), and 9(c), respectively. Fig. 9(d) shows the image of the same scene reconstructed

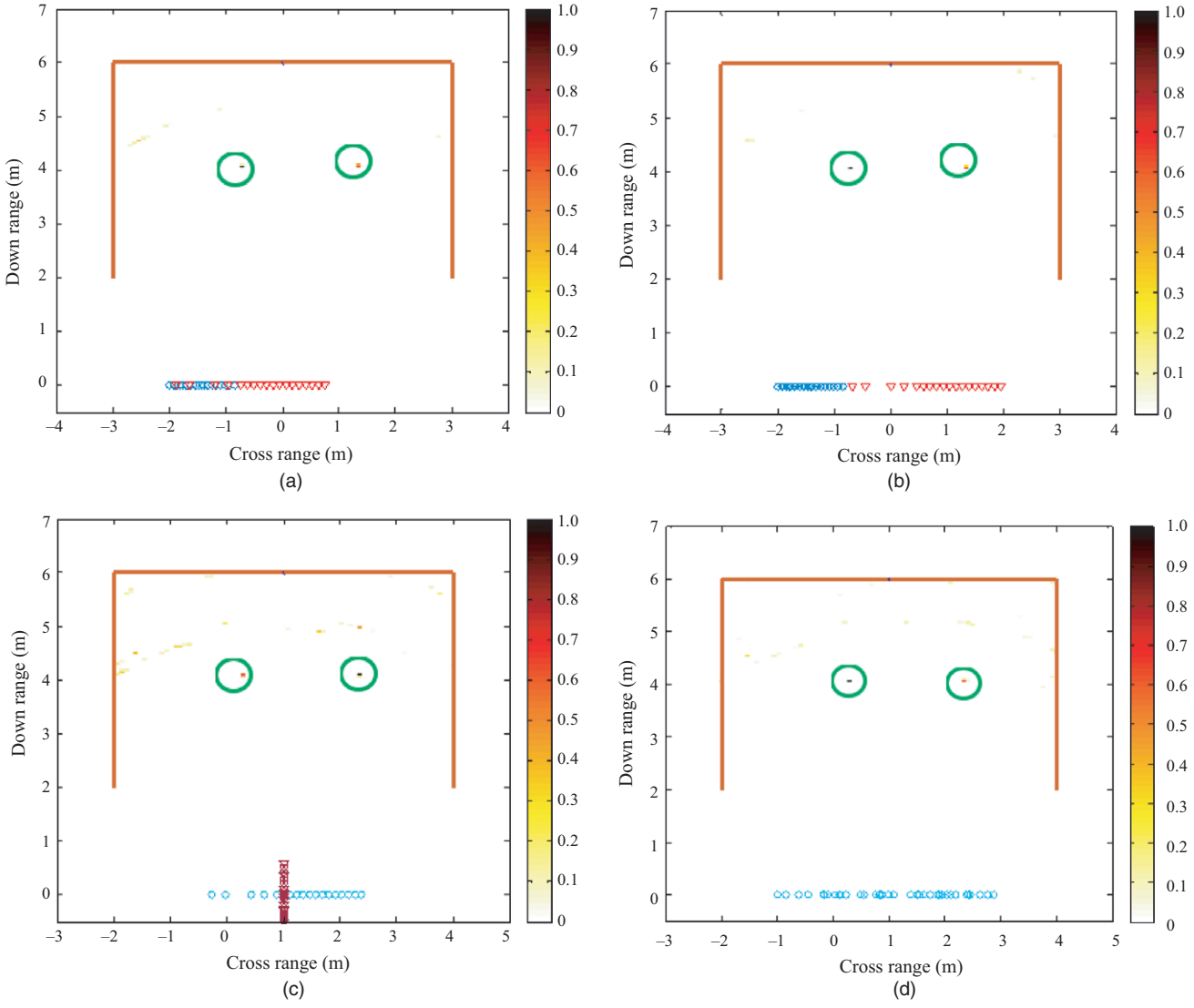

Fig. 9. Images using Pythagorean-based apertures: (a) PISA, (b) PDSA, (c) SOCA, and (d) Random CS.

https://doi.org/10.4218/etrij.2017-0241

using random CS for the purpose of comparison. From the results, the PDSA demonstrated superior performance compared to the PISA and SOCA configurations.

VII. Performance Comparison

As the application of CS to TWRI has changed the field dramatically, we can broadly categorize ghost suppression methods into two groups: multipath-exploitation-based and AD-based methods. In terms of the image quality, the results show that the former can achieve an SCR and clutter peak (RCP) of 95 dB and 25 dB, respectively, using the joint nonoverlapping group sparse approach, while the latter can attain an SCR and RCP of 97.3 dB and 23.7 dB, respectively. In terms of the computational complexity, multipath-exploitation-based approaches require a large sensing matrix to accommodate multipath returns; hence, the processing time will be relatively high. AD-based approaches, on the other hand, are computationally efficient but suffer a high probability of misses due to subimage combination.

VIII. Conclusion

TWRI is among the growing fields owing to its diverse applications. High-resolution images help during rescue missions in the case of fires and earthquakes or in hijacked building tragedies. The field is, however, challenged by multipath propagation, which reduces the probability of correct target detection, if it is not properly dealt with. This paper presented a comparative review of multipath ghost suppression in TWRI. The article started with a description of a through-the-wall radar scene, elaborating the setup and possible signal models. We enumerated the most common ghost suppression techniques: with and without multipath exploitation and those exploiting ghost characteristics. Their pros and cons were discussed to excite healthy contributions. The emphasis of the article was in the imaging of a sparse scene with a UWB signal, allowing the application of CS. It was found that a more efficient multipath ghost suppression technique which is preprocess-based is needed to properly utilize the power of CS.

Acknowledgements

This work was supported by the National Plan for Science, Technology and Innovation (Maarifah) of the Science and Technology Unit at King Fahd University of Petroleum and Minerals (KFUPM), Dhahran, Saudi Arabia (15-ELE4651-04, Multipath Exploitation in Through the Wall Radar Imaging with UWB Sparse Signals).

References

[1] M.G. Amin, *Through-the-Wall Radar Imaging*, "Boca Raton, FL, USA: CRC Press, 2010.

[2] A.T. Abdalla, A.H. Muqaibel, and S. Al-Dharrab, "Aspect Dependent Multipath Ghost Suppression in TWRI under Compressive Sensing Framework," *Int. Conf. Commun. Signal Process. Their Applicat.*, Sharjah, United Arab Emirates, Feb. 17–19, 2015, pp. 1–6.

[3] M. Leigsnering, M.G. Amin, F. Ahmad, and A.M. Zoubir, "Multipath Exploitation and Suppression for SAR Imaging of Building Interiors: An Overview of Recent Advances," *IEEE Signal Process. Mag.*, vol. 31, no. 4, 2014, pp. 110–119.

[4] D.L. Donoho, "Compressed Sensing," *IEEE Trans. Inform. Theory*, vol. 52, no. 4, Apr. 2006, pp. 1289–1306.

[5] D. Needell and A. Tropp, "CoSaMP: Iterative Signal Recovery from Incomplete and Inaccurate Samples," *Appl. Comput. Harmonic Anal.*, vol. 26, no. 3, 2009, pp. 301–321.

[6] T.Y. Al-Naffouri and M. Masood, "Distribution Agnostic Bayesian Recovery of Sparse Signals," *Int. Workshop Syst. Signal Process. Their Applicat.*, Algiers, May 12–15, 2013, pp. 283–290.

[7] P. Setlur, M. Amin, F. Ahmad, and S. Member, "Multipath Model and Exploitation in Through-the-Wall and Urban Radar Sensing," *IEEE Trans. Geosci. Remote Sens.*, vol. 49, no. 10, 2011, pp. 4021–4034.

[8] P. Setlur, G. Alli, and L. Nuzzo, "Multipath Exploitation in Through-Wall Radar Imaging via Point Spread Functions," *IEEE Trans. Image Process.*, vol. 22, no. 12, 2013, pp. 4571–4586.

[9] M.J. Oyan, S.-E. Hamran, L. Hanssen, T. Berger, and D. Plettemeier, "Ultrawideband Gated Step Frequency Ground-Penetrating Radar," *IEEE Trans. Geosci. Remote Sens.*, vol. 50, no. 1, 2012, pp. 212–220.

[10] W. Zhang, M.G. Amin, F. Ahmad, A. Hoorfar, and G.E. Smith, "Ultrawideband Impulse Radar Through-the-Wall Imaging with Compressive Sensing," *Int. J. Antennas Propag.*, vol. 2012, 2012, pp. 251497:1–251497–11.

[11] A. Muqaibel, A. Abdalla, M. Alkhodary, S, and Al-Dharrab, "Aspect-dependent efficient multipath ghost suppression in TWRI with sparse reconstruction," *Int.J.Microw.Wireless Technol.*, vol. 9, no. 9, 2017, pp. 1839–1852. doi:10.1017/S1759078717000666

[12] A.T. Abdalla, "Aspect Dependent Efficient Multipath Ghost Suppression in TWRI with Compressive Sensing," Ph.D. thesis, King Fahd University of Petroleum and Minerals, Saudi Arabia, 2016.

[13] L. Wang and X. Huang, "Research on UWB SAR Image Formation with Suppressing Multipath Ghosts," *CIE Int. Conf. Radar*, Shanghai, China, Oct. 16–19, 2006, pp. 1.

[14] Q. Tan, "A New Method for Multipath Interference Suppression in Through-the-Wall UWB Radar Imaging," *Int. Conf. Adv. Comput. Contr.*, Shenyang, China, Mar. 27–29, 2010, pp. 535–540.

[15] F.F. Wang, Y.R. Zhang, and H.M. Zhang, "Study on Through-Wall Propagation Properties of UWB Signal," . . . Posts . . ., 2013.

[16] Z. Li, L. Kong, Y. Jia, Z. Zhao, and F. Lan, "A Novel Approach of Multi-path Suppression Based on Sub-aperture Imaging in Through-Wall-Radar Imaging," *IEEE Radar Conf. (RADAR)*, Ottawa, Canada, Apr. 29–May 3, 2013, pp. 4–7.

[17] M.G. Amin and F. Ahmad, "Compressive Sensing for Through-the-Wall Radar Imaging," *J. Electron. Imaging*, vol. 22, no. 3, July 2013, pp. 30901:1–30901:21.

[18] Q. Tan, H. Leung, Y. Song, and T. Wang, "Multipath Ghost Suppression for Through-the-Wall Radar," *IEEE Trans. Aerospace Electron. Syst.*, vol. 50, no. 3, 2014, pp. 2284–2292.

[19] A.H. Muqaibel, A.T. Abdalla, M.T. Alkhodary, and S. Al-Dharrab, "Aspect-Dependent Efficient Multipath Ghost Suppression in TWRI with Sparse Reconstruction," *Int. J. Microw. Wireless Tech.*, vol. 9, no. 9, 2017, pp. 1–14.

[20] H. Mansour and D. Liu, "Blind Multi-path Elimination by Sparse Inversion in Through-the-Wall-Imaging," *IEEE Int. Workshop Comput. Adv. Multi-Sensor Adaptive Process.*, St. Martin, France, Dec. 15–18, 2013, pp. 256–259.

[21] M. Leigsnering, F. Ahmad, M. Amin, and A. Zoubir, "Multipath Exploitation in Through-the-Wall Radar Imaging using Sparse Reconstruction," *IEEE Trans. Aerospace Electron. Syst.*, vol. 50, no. 2, 2014, pp. 920–939.

[22] J. Wang, P. Wang, Y. Li, Q. Song, and Z. Zhou, "A Multipath Suppression Technique for Through-the-Wall Radar," *IEEE Int. Conf. Ultra-Wideband*, Sydney, Australia, Sept. 15–18, 2013, pp. 215–220.

[23] G. Gennarelli and F. Soldovieri, "A Linear Inverse Scattering Algorithm for Radar Imaging in Multipath Environments," *IEEE Geosci. Remote Sens. Lett.*, vol. 10, no. 5, 2013, pp. 1085–1089.

[24] G. Gennarelli, I. Catapano, and F. Soldovieri, "RF/Microwave Imaging of Sparse Targets in Urban Areas," *IEEE Antennas Wireless Propag. Lett*, vol. 12, 2013, pp. 643–646.

[25] G. Gennarelli and F. Soldovieri, "Multipath Ghosts in Radar Imaging: Physical Insight and Mitigation Strategies," *IEEE J. Sel. Top. Appl. Earth Obs. Remote Sens.*, vol. 8, no. 3, 2015, pp. 1078–1086.

[26] J. Moura and Y. Jin, "Time Reversal Imaging by Adaptive Interference Canceling," *IEEE Trans. Signal Process.*, vol. 56, no. 1, 2008, pp. 233–247.

[27] A.H. Muqaibel, A.T. Abdalla, M.T. Alkhodary, and S.A. Alawsh, "Through-the-Wall Radar Imaging Exploiting Pythagorean Apertures with Sparse Reconstruction," *Digital Sig. Process. A Rev. J.*, vol. 61, 2017, pp. 86–96.

Abdi T. Abdalla received a BS degree in electronic science and communication, and an MS degree in electronics engineering and information technology from the University of Dar es Salaam, Tanzania, in 2006 and 2010, respectively, and a PhD degree from King Fahd University of Petroleum and Minerals (KFUPM), Saudi Arabia, in 2016. Currently, he is a lecturer at the Department of Electronics and Telecommunication Engineering of University of Dar es Salaam. His research interests include through-the-wall radar imaging, indoor target localization, sparse array processing, and the application of compressive sensing to signal processing.

Mohammad T. Alkhodary received his MSc and PhD degrees form from King Fahd University of Petroleum and Minerals, Dhahran, Saudi Arabia, in 2012 and 2017 respectively. He is now working as a postdoc at École de technologie supérieure, Montreal, Canada. His research interests include signal processing for radar imaging, UWB communication, and compressive sensing theory and applications.

Ali H. Muqaibel received his BS and MSc degrees from King Fahd University of Petroleum and Minerals (KFUPM), Dhahran, Saudi Arabia, in 1996 and 1999, respectively, and a PhD degree from Virginia Polytechnic Institute and State University, Blacksburg, VA, USA in 2003. He is currently the director of the Telecommunications Research Laboratory and an associate professor with the Electrical Engineering Department, KFUPM. His main areas of interest include ultrawideband signal processing for localization and communications.

https://doi.org/10.4218/etrij.2017-0241